https://doi.org/10.2352/ISSN.2470-1173.2020.10.IPAS-179


# Hyperspectral complex-domain image denoising: cube complex-domain BM3D (CCDBM3D) algorithm

*Vladimir Katkovnik, Mykola Ponomarenko, Karen Egiazarian, Igor Shevkunov and Peter Kocsis*
*Tampere University, FIN 33101, Tampere, Finland*

## Abstract

*We consider hyperspectral phase/amplitude imaging from hyperspectral complex-valued noisy observations. Block-matching and grouping of similar patches are main instruments of the proposed algorithms. The search neighborhood for similar patches spans both the spectral and 2D spatial dimensions. SVD analysis of 3D grouped patches is used for design of adaptive nonlocal bases. Simulation experiments demonstrate high efficiency of developed state-of-the-art algorithms.*

*Keywords: Block matching, Complex domain, Denoising, Hyperspectral imaging, Sparsity*

## Introduction

Recently, hyperspectral imaging (HSI) is a hot topic in many application and research fields, such as earth surface remote sensing [1], medical and bio-medical sciences [2], etc. Typically, HIS retrieves a valuable information based on images obtained across a wide range of electromagnetic spectrum with hundreds to thousands of spectral channels. These images are two-dimensional (2*D*) and stacked together in 3*D* cubes, where (*x,y*) are spatial coordinates and the third coordinate is for the spectral channel, which usually is represented by wavelength λ.

A flow of publications are targeted on HSI, and the sparsity concept is one of the leading instruments for the topic (e.g. [3]). However, these papers are mainly restricted to real-valued data.

The complex domain HSI makes a special class of the hyperspectral problems since variables of interest are complex-valued and both phase and amplitude have to be reconstructed. It is a very promising technique which doubles amount of retrieved information in comparison with the real-valued HSI, since measured hyperspectral cubes are complex-valued, i.e. each of 2*D* images for each wavelength is complex-valued having 2*D* phase and amplitude.

The complex-valued data cubes may appear as the Fourier transform of observed real-valued variables (e.g. [4]) or as direct measurements of real and imaginary parts of complex-valued parameters. For instance, in magnetic resonance imaging (MRI) and functional magnetic resonance imaging (fMRI), images or voxel measurements are complex-valued (e.g.[5]).

Recently, hyperspectral (HS) holography has been developed, which, additionally to the conventional holography, is able to recover a spectrally resolved phase information (e.g. [6, 7]).

An important point in HSI is that the corresponding HS cubes are derived usually from indirect observations as solutions of inverse problems, what leads to serious noise amplification. A sliding window averaging along the wavelength dimension is used routinely for noise suppression (e.g. [6,7]), but this approach may result in oversmoothing of estimated signals. Application of more sophisticated algorithms with separate filtering of phase and amplitude for each wavelengths has appeared as a more efficient instrument in HSI [8].

Novel effective denoising algorithms taking into consideration phase/amplitude correlation between and within slices of HS cubes are proposed and studied in [9, 10]. In these algorithms, the observed noisy complex-valued 3D cubes are analyzed based on SVD. A small number of eigenimages obtained in this analysis are filtered by Complex Domain Block-Matching Three Dimension (CDBM3D) filters [11-13], which are a complex domain development of the well known sparsity based BM3D techniques [14]. The filtered eigenimages allow to reconstruct the filtered 3D cubes.

A different approach to denoising of 3D cubes is proposed in this paper based on the sparsity techniques developed for complex domain data. It is an extension for complex domain of the BM3D video-filtering (VBM3D) [15]. A structure of the proposed algorithms is quite similar to the structure of the CDBM3D filters [11-13] with the main difference concerning the grouping of similar 2D patches.

We realize this grouping by 3D block-matching, a procedure that tests the similarity inside the reference block as well as between the reference block and blocks that belong to a search neighborhood. Given the nature of hyperspectral data, the search neighborhood is a 3D domain that spans both the spectral and 2D spatial dimensions.

Note that in CDBM3D, the grouping is restricted to 2D spatial dimension.

We demonstrate the visual and numerical advantage of the new algorithms with respect to CDBM3D as well as the much more advanced algorithms developed in [9] specifically for HSI. This advantage is gained at the price of more demanding computations.

## Problem formulation

Let $U(x,\lambda) \subset \boldsymbol{C}^{NxM}$ be a slice $N$ x $M$ on $x$ ($x$ is given on $N$ x $M$ integer grid) of a complex-valued hyperspectral cube provided a fixed wavelength λ, and $Q_\Lambda(x) = \{U(x,\lambda), \lambda \subset \Lambda\}$, $Q_\Lambda \subset \boldsymbol{C}^{NxMxL_\Lambda}$ be the whole cube composed of the set of the wavelength slices $\Lambda$ with number of the individual wavelengths $L_\Lambda$.

The total size of the cube is $N$ x $M$ x $L_\Lambda$ pixels. The third dimension rows of $Q_\Lambda(x)$ contain $L_\Lambda$ spectral observations corresponding to the scene with fixed a coordinate $x$. Then, the noisy HS observations with the additive noise may be written as:

$$Z_\Lambda(x) = Q_\Lambda(x) + \varepsilon_\Lambda(x), \qquad (1)$$

where $Z_\Lambda$, $Q_\Lambda$, $\varepsilon_\Lambda \subset \boldsymbol{C}^{NxMxL_\Lambda}$ represent noisy HS data, clean HS and additive noise, respectively.

Accordingly to the notation for the clean image, the noisycube can be represented as $Z_\Lambda(x) = \{Z(x,\lambda), \lambda \in \Lambda\}$, $Z_\Lambda \subset \boldsymbol{C}^{NxMxL_\Lambda}$ with the slices $Z(x, \lambda)$.

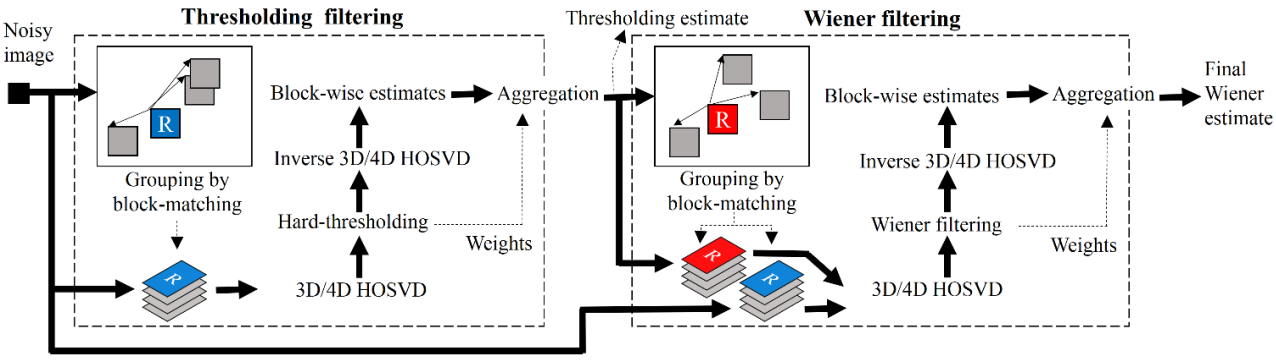


*Figure 1. The flowchart of the proposed complex domain algorithms*

The denoising problem is formulated as a reconstruction of unknown $Q_A(x)$ from the given noisy $Z_A(x)$.

The properties of the clean HS cube $Q_A(x)$ and the noise $\varepsilon_A(x, y)$ are essential for the algorithm development.

The following three assumptions are basic hereafter.

1) *Similarity* of the HS slices $U(x, \lambda)$ for close values of $\lambda$ follows from the fact that usually the slides $U(x, \lambda)$ are slowly varying on $\lambda$.

2) *Sparsity* of 2D images $U(x, \lambda)$ as functions of $x$ means that there are bases such that $U(x, \lambda)$ can be represented with a small number of atoms. It is one of the natural and fundamental assumptions for design of modern image processing algorithms. The sparsity for complex-valued images is quite different from the standard formulation of this concept for real-valued signals. The complex-valued variables can be defined by any of two pairs: amplitude/phase or real/imaginary values and elements of these pairs usually are correlated [11]. Thus, the sparsity can be introduced for different variables: directly for complex-valued or for the real-valued pairs: amplitude/phase or real/imaginary.

3) The noise $\varepsilon_A(x)$ is zero mean circular Gaussian.

## Proposed algorithms

The concept of non-local grouping and collaborative filtering is extensively studied (e.g. in [14], [11], [12], [13]. In this section, we provide a brief overview of the basic steps of this concept in connection with the proposed filtering of the 3D cube data composed from multiple slices.

The first step of the algorithm is 'grouping'. For each pixel of the slice, called the reference pixel, we define a small 2D square patch (block), reference slice (block), and look for similar patches inside the slice of the reference patch and within other neighboring slices. The similar 2D patches are stacked together and form 3D arrays-groups. It defines the abbreviation BM3D where 3D stands for the dimension of groups.

The second step is 'collaborative' filtering. We are looking for the best adaptive bases for sparse representation of the groups. The High-Order SVD (HOSVD) is used for the group analysis, which gives the orthonormal transforms of the grouped data. The filtering of the groups is produced in the transform domains defined by these orthonormal transforms. The small coefficients of these transforms are thresholded (put to zero), i.e. the hard-thresholding procedure. The soft thresholding can be used at this step. The inverse transform applied to the filtered transform domain groups returns the filtered image domain groups.

The collaborative filtering is produced successively taking all pixels of the cube as the reference pixels. Thus, it can be reference pixels and patches from all slices. Of course, computationally, it can be too demanding. To be realistic, we take the reference pixels and the reference slices with some steps, similar as it is done in BM3D implementations.

The third step is 'aggregation'. The patches collected in the filtered groups are returned to their original positions, where from they were taken for this group. As a result, for each pixel of the cube we gain multiple estimates obtained due to the reference patches from the slide where this pixel is located as well as due to the reference patches from other slices.

The aggregation defines the pixel-wise estimate as a weighted mean of all estimates available for this pixel. As the thresholding is used for filtering, this estimate is called the final thresholding estimate. In this way, the estimates for all slices are tightly connected with each other.

The proposed algorithm similar to the standard BM3D as in [14] is composed from two stages. The first one is the thresholding stage by the name of the used filtering.

The second stage differs by the filtering procedure produced in the HOSVD transform domain. Instead of the thresholding, we use the Wiener filtering also produced in the transform domain and the stage is called the Wiener filtering stage.

The algorithm flowchart, composed from the two successive stages of thresholding and Wiener filtering, is shown in Fig.1.

The variety of the CDBM3D algorithms are presented in Complex Domain Image Denoising (CDID) Toolbox in [13] is defined by different sparsity models in complex domain:

(I) Straightforward complex domain sparsity treating variables as complex-valued;

(II) Sparsity imposed of real and imaginary parts of complex-valued variables;

(III) Sparsity imposed on amplitude and phase of complexvalued variables.

HOSVD is applied for analysis and synthesis of grouped data. This is 3D HOSVD for the sparsity model I and 4D HOSVD for the sparsity models II and III.

All these three sparsity models are used in our algorithms for HSI. Thus, a variety of the algorithms for HSI are presented and studied in this paper.

The structural image Fig.1 looks identical to the flowchart in [11], [13] but as it is already mentioned above the algorithms in this paper are different by the grouping rules, selecting similar patches not only in the reference slice of HS data but in the neighboring slices different by spectral coordinate, as well as by the aggregation of estimates obtained after processing different 3D groups.

*Figure 3. Channel #25 of test image: a) true phase, b) true amplitude, c) noisy phase, σ=0.5, $SNR_\varphi$ = 0.7 dB, d) noisy amplitude, e) BM4D, $SNR_\varphi$ = 13.3 dB, f) CCF, $SNR_\varphi$ = 16.2 dB, g) ImRe-BM3D WI, $SNR_\varphi$ = 19.6 dB, h) ImRe-BM3D IT, $SNR_\varphi$ = 20.9 dB*

The input/output link given by the proposed algorithms can be presented in the form:

$$\hat{Q}_\Lambda(x) = CCDBM3D\{Z_\Lambda(x)\}, \quad (2)$$

where CCDBM3D stands for Cube Complex Domain Block-Matching 3D filter, $\hat{Q}_\Lambda(x)$ is an estimate of the true cube $Q_\Lambda(x)$ and $Z_\Lambda(x)$ is a cube of noisy observations.

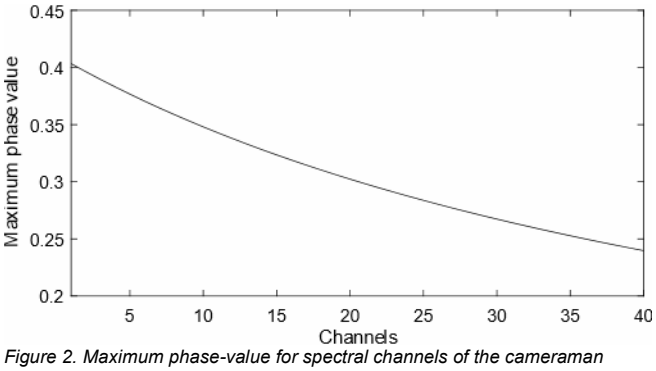


*Figure 2. Maximum phase-value for spectral channels of the cameraman phase test-image*

The accuracy analysis produced for the CCDBM3D algorithms proves that the best results are obtained by the sparsity model II using real and imaginary parts of random variables for the analysis and synthesis procedures. In the following tests we shown CCDBM3D results obtained by the algorithm using real/imaginary sparsity modeling.

We compare two versions of this algorithm:

(1) Implemented according to the flowchart Fig.1 with Wiener filtering (ImRe-BM3D WI);

(2) Iterative version of this algorithm (ImRe-BM3D IT), see [13].

As the state-of-the-art counterpart algorithm, we use the recent Complex domain Cube Filter (CCF) based on SVD analysis of the total cube of HS observations and CDBM3D filtering in the reduced size SVD eigenspaces [9].

For comparison, we show also the results obtained by the BM4D algorithm what is an extension of the BM3D filter to volumetric data (BM4D) [16]. In our problem, the volumetric data means 3D HS cube. This algorithm implements the grouping and collaborative filtering paradigm, where mutually similar 3D-dimensional patches are stacked together in a 4D groups jointly filtered in transform domain contrary to 3D groups implemented in BM3D.

BM4D is the state-of-art algorithm for real-valued HS data. In our tests, we apply it for denoising of phase of 3D HS cube complex-valued observations.

## Comparative analysis for simulated HS data

Simulation experiments are produced for the complex-valued HS cube of a transparent phase object. The phase delay of this object is described by the equation:

$$\varphi_\lambda(x,y) = 2\pi\frac{h(x,y)}{\lambda}(n_\lambda - 1), \quad (3)$$

where $\lambda$ is a wavelength of a laser radiation going through the object, $n_\lambda$ is the refractive index of an object material and $h(x, y)$ is a thickness of the object.

We model the HS cube for this object by 40 slices uniformly covering the wavelength interval $\Lambda$ = [427…707] *nm*. The MATLAB cameraman test-image is used for $h(x, y)$ to model a phase-delay of the object. It is scaled in such way that the phase

delay maximal for each slice belongs to the interval [0 … 0.4] radians (see Fig. 2).

The amplitude of the object transfer function (object transparency) varying in $(x, y)$ is inverse proportional to the object thickness $h(x, y)$ scaled with the minimal value equal to 1, and the mean value equal to 10. About this kind of varying amplitude modeling see [11, 13]. The amplitude is the same for all spectral slices of HS data.

The amplitude and phase images for the spectral channel #25, $\lambda = 595$ *nm*, as examples of phase and amplitude, are shown on the Fig. 3.

Noisy images are formed by adding noise to real and imaginary components of each channel according to Eq.(1). One should note that this noise is additive to amplitude and signal depended for observed phase (the noise variance is inversely proportional to amplitude). The goal of our analysis is phase imaging, i.e. quality restoration of the true phase ' from the noisy data comparing the algorithms. For the interferometric phase, the accuracy of phase restoration is measured by the signal-to-noise ratio (SNR):

$$SNR_{\varphi} = 10\log_{10}\frac{\left\|\varphi_0 - \overline{\varphi}_0\right\|_2^2}{\left\|W(\hat{\varphi}_0 - \varphi_0)\right\|_2^2}[dB], \qquad (4)$$

where $\hat{\varphi}_0$ and $\varphi_0$ are the phase reconstruction and the true phase, respectively; $\overline{\varphi}_0$ is mean level of the true phase; the phase wrapping operator $W$ is used in order to eliminate erroneous phase shifts multiple to $2\pi$.

The phase denoising results for channel #25, $\sigma = 0.5$, are shown in Fig. 3. The BM4D algorithm working directly in the phase domain does not take into account signal dependent nature of the noise. As a result, some areas of phase images are oversmoothed while others contain quite visible residual noise. Numerically, BM4D is worst with the smallest $SNR\varphi$. The best accuracy is demonstrated by the proposed ImRe-BM3D IT and ImRe-BM3D WI algorithms with a slightly better result for the iterative ImRe-BM3D IT. These algorithms significantly outperform CCF by about 3 dB.

Let $SNR\varphi(k, m)$ be a set of $SNR\varphi$ calculated for $k \in K$, $m \in M$, where $K$ and $M$ denote the sets of the algorithms and 40 spectral channels, respectively.

The best algorithm for each channel is defined as

$$mSNR_{\varphi}(m) = \max_{k \in K} SNR_{\varphi}(k, m). \qquad (5)$$

We compare the algorithms with respect to these best results using differences between the corresponding SNRs:

$$\Delta SNR_{\varphi}(k, m) = SNR_{\varphi}(k, m) - mSNR_{\varphi}(m). \qquad (6)$$

Box-plots of $\Delta SNR_{\varphi}(k,m)$ being depicted for each algorithm (each $k$) gives comparative statistics for evaluation of the algorithm's performance for all channels (all $m$).

Box-plots on the Fig. 4 show $\Delta SNR_{\varphi}$ for $\sigma = 1$. It is clearly seen that for all channels the best results are provided by ImRe-BM3D IT, which outperforms ImRe-BM3D WI on 1 dB, CCF on 4 dB, BM4D on 8 dB as compared with the median, middle ('red') lines in the boxes.

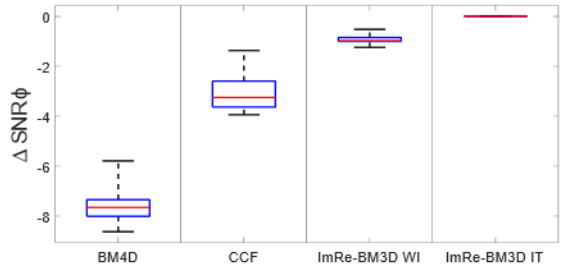


*Figure 4. Box-plots for the compared algorithms, σ = 1*

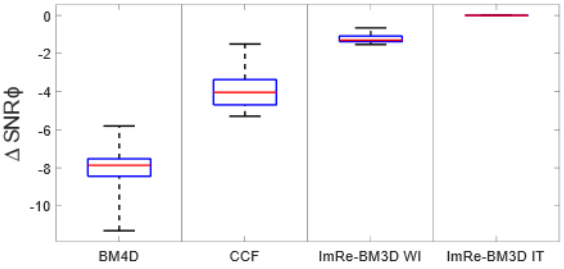


*Figure 5. Box-plots for the compared algorithms, σ = 0.5*

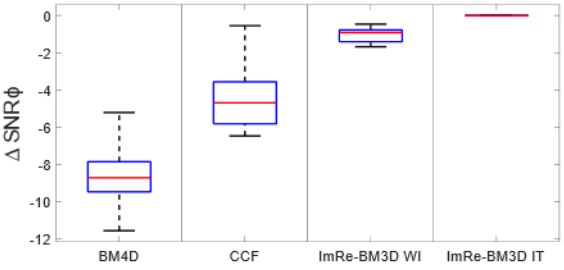


*Figure 6. Box-plots for the compared algorithms, σ = 0.25*

Fig. 5 and Fig. 6 show box-plots for $\sigma = 0.5$ and $\sigma = 0.25$. The best algorithm is the same, however, with smaller $\sigma$ the gap between $SNR_{\varphi}$ for the different algorithms is decreased.

## Comparative analysis for measured data

The object of study is a transparent binary phase mask manufactured for lensless imaging. Phase and amplitude transfer functions of this object, shown in Fig. 7, have been measured in our experiments using off-axis interferometry for three wavelengths $\lambda = 402$ *nm*, $\lambda = 532$ *nm* and $\lambda = 643$ *nm*. Five additional measurements for $\lambda$ = [407, 412, 417, 422, 527] *nm* are obtained numerically by interpolation. We treat these data as a true HS complex-valued cube $Q_M(x)$ of 8 spectral channels.

Fig. 8 shows maximum values of phase for each of the channels. One can see that there is a large phase deviations between the channels 5, 6 and 7, 8.

The noisy data corresponding to this object are generated according to Eq. (1) and used for comparison of the algorithms.

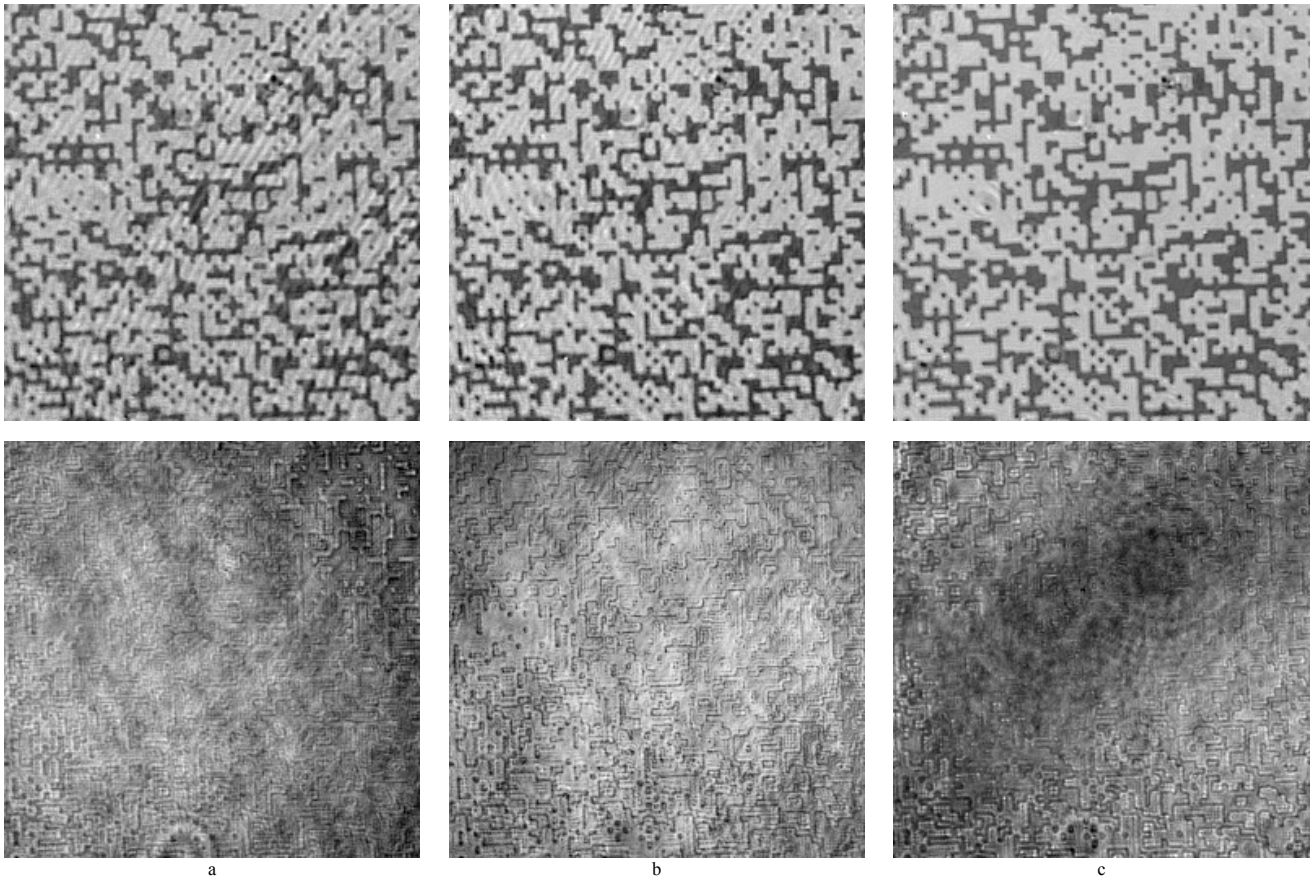

a b c

*Figure 7. Three spectral images of the binary phase mask: a) phase (above) and amplitude (bellow) for λ = 402 nm, b) phase and amplitude for λ = 532 nm, c) phase and amplitude for λ = 643 nm*

The large deviations in phase noticed above make denoising difficult as neighbouring slices of the HS cube may be too different for joint using in block-matching denoising.

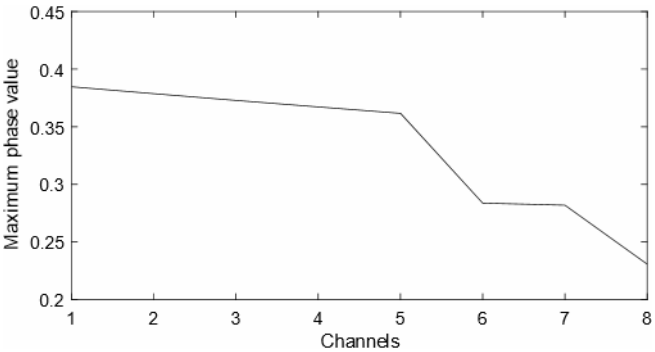


*Figure 8. Maximum phase value for channels of the test image*

The denoising results as *SNRφ* curves are shown on the Fig. 9 for $\sigma = 0.06$. It is clearly seen that CCF fails on the channels 6, 7 and 8, and the best results are achieved by the proposed two algorithms.

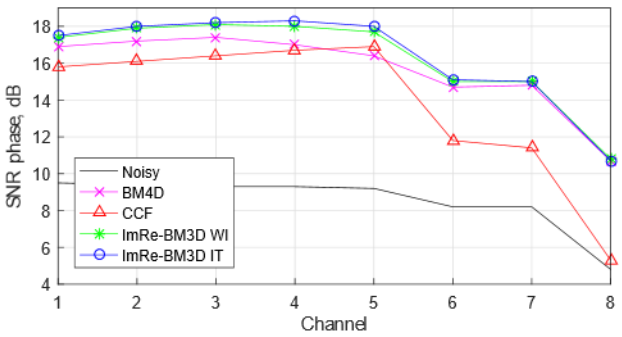


*Figure 9. SNRφ for compared algorithms, σ = 0.06.*

Finally, box-plots for all channels and all noise standard deviations ($\sigma = 0.03, 0.06, 0.15, 0.3$) are shown on Fig. 10.

The best accuracy is provided by ImRe-BM3D WI slightly outperforming ImRe-BM3D IT. BM4D is behind them in average on 0.5 dB. CCF provides significantly lower values of *SNRφ*.

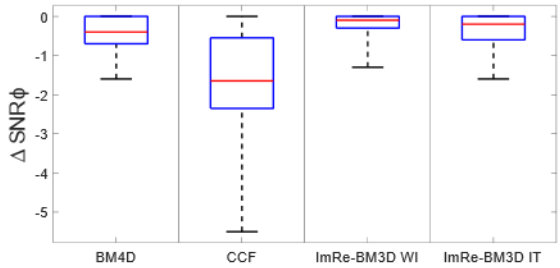


*Figure 10. Box-plots for all channels and all noise standard deviations σ = {0.03, 0.06, 0.15, 0.3}*

## Conclusions

In this paper, we present the novel algorithms for denoising of HS complex-valued observations. In simulation experiments, the algorithms demonstrate the state-of-the-art performance visually and numerically mainly owing to the novel block-matching of similar patches and SVD analysis/synthesis based joint modeling of real and imaginary parts of complex-valued variables. The MATLAB demo-version of the CCDBM3D algorithms is publicly available on http://www.cs.tut.fi/sgn/imaging/sparse/ccdbm3d.zip.

## Acknowledgement

This work is supported by the Academy of Finland, project no. 138207, 2015-2019.

## References

[1] M. J. Khan, H. S. Khan, A. Yousaf, K. Khurshid, and A. Abbas, "Modern Trends in Hyperspectral Image Analysis: A Review," pp. 14 118–14 129, 2018.

[2] G. Lu and B. Fei, "Medical hyperspectral imaging: a review," Journal of Biomedical Optics, vol. 19, no. 1, p. 010901, 2014.

[3] R. M. Willett, M. F. Duarte, M. A. Davenport, and R. G. Baraniuk, "Sparsity and structure in hyperspectral imaging: Sensing, reconstruction, and target detection," IEEE signal processing magazine, vol. 31, no. 1, pp. 116–126, 2013.

[4] M. S. Kulya, V. A. Semenova, V. G. Bespalov, and N. V. Petrov, "On terahertz pulsed broadband Gauss-Bessel beam free-space propagation," Scientific Reports, vol. 8, no. 1, p. 1390, 12 2018.

[5] D. B. Rowe, "Modeling both the magnitude and phase of complexvalued fMRI data," NeuroImage, vol. 25, no. 4, pp. 1310–1324, 2005.

[6] S. G. Kalenkov, G. S. Kalenkov, and A. E. Shtanko, "Hyperspectral holography: an alternative application of the Fourier transform spectrometer," Journal of the Optical Society of America B, vol. 34, no. 5, p. B49, 2017.

[7] D. Claus, G. Pedrini, D. Buchta, and W. Osten, "Accuracy enhanced and synthetic wavelength adjustable optical metrology via spectrally resolved digital holography," Journal of the Optical Society of America A: Optics and Image Science, and Vision, vol. 35, no. 4, pp. 546–552, 2018.

[8] G. S. Kalenkov, S. G. Kalenkov, I. G. Meerovich, A. E. Shtanko, and N. Y. Zaalishvili, "Hyperspectral holographic microscopy of bio-objects based on a modified Linnik interferometer," Laser Physics, vol. 29, no. 1, p. 016201, 1 2019.

[9] I. Shevkunov, V. Katkovnik, D. Claus, G. Pedrini, N. Petrov, and K. Egiazarian, "Hyperspectral phase imaging based on denoising in complex-valued eigensubspace," submitted to Optica, 2019.

[10] V. Katkovnik, I. Shevkunov, and K. Egiazarian, "Hyperspectral complex domain imaging from complex domain noisy observations," submitted to EUSIPCO 2019, pp. 1–5, 2019.

[11] V. Katkovnik, M. Ponomarenko, and K. Egiazarian, "Sparse approximations in complex domain based on BM3D modeling," Signal Processing, vol. 141, pp. 96–108, 12 2017.

[12] V. Katkovnik and K. Egiazarian, "Sparse phase imaging based on complex domain nonlocal BM3D techniques," Digital Signal Processing: A Review Journal, vol. 63, pp. 72–85, 2017.

[13] V. Katkovnik, M. Ponomarenko, and K. Egiazarian, "Complex-valued image denosing based on group-wise complex-domain sparsity," Arxiv, pp. 1–36, 11 2017. [Online]. Available: http://arxiv.org/abs/1711.00362

[14] K. Dabov, A. Foi, V. Katkovnik, and K. Egiazarian, "Image Denoising by Sparse 3-D Transform-Domain Collaborative Filtering," IEEE Transactions on Image Processing, vol. 16, no. 8, pp. 2080–2095, 8 2007.

[15] K. Dabov, A. Foi, and K. Egiazarian, "Video denoising by sparse 3d transform-domain collaborative filtering," in 2007 15th European Signal Processing Conference. IEEE, 2007, pp. 145–149.

[16] M. Maggioni, V. Katkovnik, K. Egiazarian, and A. Foi, "Nonlocal transform-domain filter for volumetric data denoising and reconstruction," IEEE transactions on image processing, vol. 22, no. 1, pp. 119– 133, 2012.

# JOIN US AT THE NEXT EI!

IS&T International Symposium on

# Electronic Imaging

SCIENCE AND TECHNOLOGY

*Imaging across applications . . . Where industry and academia meet!*

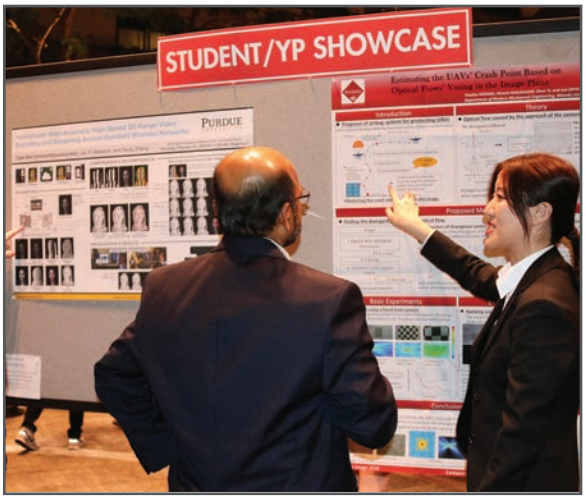


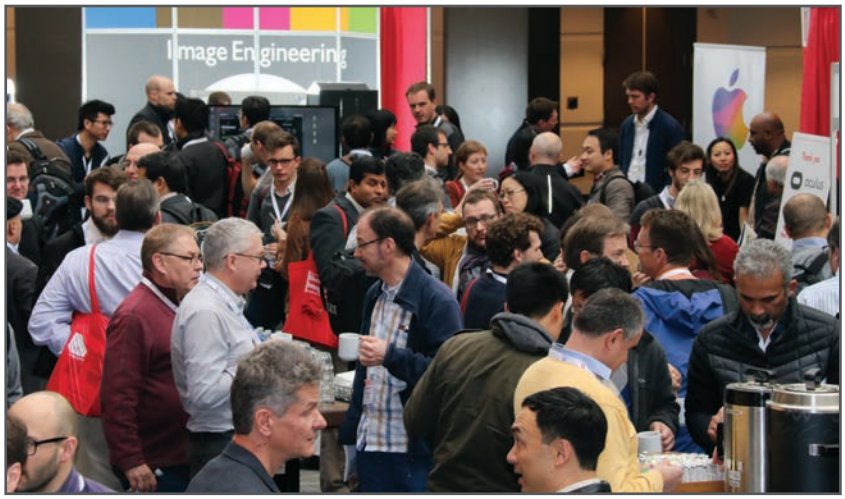



**• SHORT COURSES • EXHIBITS • DEMONSTRATION SESSION • PLENARY TALKS •**
**• INTERACTIVE PAPER SESSION • SPECIAL EVENTS • TECHNICAL SESSIONS •**

**www.electronicimaging.org**

IS&T
imaging.org